Journal of Materials Chemistry A

Accepted Manuscript

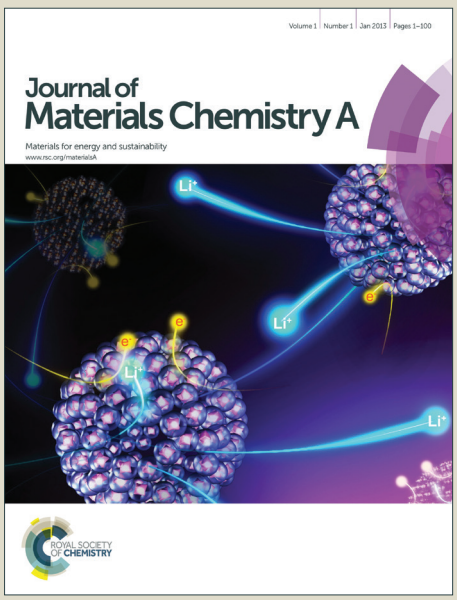

ROYAL SOCIETY OF CHEMISTRY

www.rsc.org/materialsA

Journal Name

ARTICLE

Sandwiched Graphene with Nitrogen, Sulphur co-doped CQDs: Efficient Metal Free Material for Energy Storage and Conversion Application†

Received 00th January 20xx,
Accepted 00th January 20xx

DOI: 10.1039/x0xx00000x

www.rsc.org/

Aneeya K. Samantara,[a,b] Subash Chandra Sahu,[a,b] Arnab Ghosh[c] and Bikash Kumar Jena[a,b*]

Here, a hybrid material of sandwiched reduced graphene oxides (rGO) and N, S co-doped carbon quantum dots (N, S-CQDs) was prepared following a facile synthetic route. This metal free composite has demonstrated their dual performance as electrode material for supercapacitor and fuel cell catalyst. It shows robust cyclic stability with high energy and power density without any binders. The enhanced activity of the composite can be ascribed to the substantial role of CQDs present within the interlayer of rGO to enhance the accessible for charged ions which depicts the increased capacitance of composites. In addition, the electrocatalytic activity of the composite has been assessed as metal free cathode catalyst towards the oxygen reduction reaction (ORR) for fuel cell applications. It shows better performance in terms of high reduction potential and high reduction current as compared to the rGO. This can be ascribed due to the significant contribution of electron rich heteroatom doped CQDs as well as the synergistic effect of both CQDs and rGO for electrocatalytic reduction of oxygen. The interesting dual performance of heteroatom doped CQDs and graphene hybrid composites hold potential for development of energy storage and conversion devices.

Introduction

The development of various types of electronic gadgets, portable electronic devices, and electrical vehicles demands the requirement of alternative high power energy storage and conversion devices in substitute to the traditional energy resources.[1] Fuel cells, batteries and supercapacitors are searched to be some of the substitutes. As a storage device, supercapacitor has been proved to be suitable for speedy storage and release of energy due to its higher specific capacitance, longer cycle stability and rapid charge-discharge property.[2] They are broadly used in memory backup systems for many electronic gadgets, consumer electronics etc. Therefore, substantial efforts have been paid not only to enhance the capacitance of the existing materials but also to search an easily available new electrode material with high storage efficiency.[2c]

Likewise, the energy conversion device, fuel cell is expected to be an alternative source to overcome the limitation of energy resource from fossil fuel. Therefore, the development of efficient materials for cathode and anode become an emerging challenge for the researchers to design and commercialization of fuel cells. The oxygen reduction reaction (ORR) is one of the efficient reactions occurring at the cathode of the proton exchange membrane fuel cell. Mainly the platinum, metal alloys and their supported hybrids were used as efficient material for development ORR catalysts.[3] But the surface poisoning and corrosive action of the intermediate generated during the reduction process foul such catalyst surface and decreased the efficiency. The cost and scarcity of metals demand to explore the alternate materials for ORR interest. Therefore, extensive efforts have been devoted to the development of highly active metal free electrocatalyst with robust stability and economically viable.

The abundant nature and low cost of the carbon-based materials motivate for the choice for many technology applications.[4] The new generation carbon nanomaterials have been playing the vital role in the design and development of sustainable energy storage and conversion devices.[5] Graphene, a 2D carbon material has been broadly used in electronics, for preparation of catalysts, development of sensors etc. due to its ultra-high electrical conductivity, thermal stability, chemical inertness and high surface area.[6] The graphene and its composite (with metal, metal oxides and metal sulphides) are broadly employed as the electrode material for fuel cells, batteries and supercapacitors.[7] Many strategies have been developed to tune the properties of graphene by doping with single or hetero atoms for metal free ORR applications.[8] It has been documented that the doping of graphene with electron-rich atoms increases the activity for oxygen reduction.[5a,9] However, the usual requirement of sophisticated instruments, use of toxic precursors, high-temperature methods and high-

[a] Colloids & Materials Chemistry, CSIR-Institute of Minerals and Materials Technology, Bhubaneswar-751013, India.
[b] Academy of Scientific & Innovative Research, New Delhi-110001, India.
[c] Institute of Physics, Bhubaneswar-751005, India.

†Electronic Supplementary Information (ESI) available: [UV-visible, photoluminescence, FESEM, XPS, Raman measurements, scheme showing arrangement of symmetric supercapacitor and equations used for calculation of capacitance and no of electrons involved in ORR]. See DOI: 10.1039/x0xx00000x

cost process for doping on graphene impede their facile production for the prolific use in energy conversion applications.[10] Recently, the discovery of a new generation carbon quantum dots (CQDs) with tunable properties open to exploring many applications.[11] The CQDs are the new type of luminescent materials to substitute the transition metal based quantum dots. The negligible toxicity, higher bio-compatibility and highly functionalized surface made them very much interesting towards the designing of various biological works and electronic devices.[11a,12] Unlike graphene, the facile process for doping of CQDs with heteroatom like N, S, and P, etc. creates a tremendous attention towards the enhancement of its catalytic, electronic and optical property.[13] Therefore, the hybrid of graphene and doped CQDs has been attracted for utilization in energy storage and conversion application. Few reports have been documented with the development of doped CQDs and graphene hybrids and explored their potential application as the cathode catalyst for fuel cell applications.[14] However, the synergy effect of hetero atoms doped CQDs and graphene hybrids for supercapacitor applications have not been explored thoroughly. The recent report on micro-supercapacitor application of graphene quantum dots (GQDs), supercapacitor properties of CQD-aerogel, CQDs/RuO_2 and GQDs-CNT encourages in exploring the supercapacitor performance of CQDs and graphene hybrids.[15,16] Very recently, Chen et al. portrayed the supercapacitor performance of electrochemically deposited graphene quantum dots on 3D graphene.[17]

In this work, we prepared the N, S co-doped CQDs (CQDs-HP) and their graphene composites (rGO/CQDs-HP) by following a facile, single step hydrothermal synthetic route. The dual performance of as-synthesized rGO/CQDs-HP was investigated towards supercapacitor and cathode electrocatalyst for oxygen reduction reaction. This is the first report portrays the dual performance of this rGO/CQDs-HP as electrode material for energy storage and conversion application.

Experimental Section

Materials

Graphite powder, Potassium permanganate and Hydrogen peroxide were purchased from Sigma-Aldrich. Heparin sodium, Protamine sulphate, Sodium sulphate (anhydrous), cellulose nitrate membrane (pore size of 0.22 μm), dialysis membrane (10 kDa) were collected from Himedia chemicals, India. All the chemicals of analar grade were used as received without any further purification. The deionized water (18 Ω.m) was used for the preparation of all the aqueous solutions.

Synthesis of graphene oxide (GO)

The Graphene oxide was synthesized by following the modified Hummer's method.[3b,18] Briefly, 1g of graphite powder and 25 ml of concentrated H_2SO_4 was mixed in a conical flask and stirred in an ice bath. 3.5g of $KMnO_4$ was added slowly to it with continuous stirring. Then, the solution was allowed to stir for two hours at room temperature maintained with a water bath. The solution was diluted with 50 ml of deionised water, and sufficient amount of H_2O_2 (30%) was added to it until the effervescence of gasses ceases. The brown coloured suspension was filtered and repeatedly washed with 0.1M HCl followed by deionized water for complete removal of SO_4^{2-} ions. The washed graphene oxide was ice dried by a lyophilizer and stored in a desiccator for prior use.

Synthesis of reduced graphene oxide (rGO)

A well-dispersed aqueous solution of graphene oxide was prepared by taking 10 mg of graphene oxide in 10 ml of deionised water by ultrasonication for 45 minute. The dispersed solution was transferred to a Teflon-lined stainless steel autoclave and placed inside an oven at 180°C for 24 hours. Then, the solution was filtered and washed with deionised water. The filtered sample was dried in the hot-air oven and stored for future use.

Synthesis of CQDs-HP

The carbon quantum dots were prepared by a facile hydrothermal method. Here, 0.1 percentage solution of Heparin sodium and Protamine sulphate in the ratio of 1:1 were taken in a Teflon-lined stainless steel autoclave and placed in an oven at 180 °C for 8 hours. The brown coloured solution obtained was centrifuged at 6000 rpm for 20 min to remove the larger sized particles. The supernatant was taken for dialysis against deionized water for two days at room temperature. Then, the solution was collected after dialysis and stored at 8 °C for further use. Hereafter, the carbon quantum dots synthesized by this approach is referred as CQDs-HP. Further, two different samples of CQDs are synthesized by taking 2:1, and 1:2 ratio of Heparin and Protamine, and the synthesized samples are referred as CQDs-HP (2:1) and CQDs-HP (1:2), respectively.

Synthesis of rGO/CQDs-HP

The Synthesis of the reduced graphene and CQDs-HP hybrid composite (rGO/CQDs-HP) was carried out as the procedure followed for synthesis of rGO. In a typical procedure, 10 mg of graphene oxide was dispersed in 10 ml of the aqueous solution of CQDs-HP (1:1 ratio) by sonication. The dispersed solution was transferred to a Teflon-lined stainless steel autoclave and placed at 180 °C for 24 hours. The sample was washed and separated by centrifugation. It was dried in a hot air oven and stored for future use. Further, two different samples of rGO/CQDs-HP composites are synthesized at same experimental conditions with variation of their proportion in 1:2 and 2:1 ratio of rGO and CQDs-HP respectively. Hereafter, the as-synthesized samples are referred as rGO/CQDs-HP (1:2) and rGO/CQDs-HP (2:1), respectively.

Characterization

The surface morphology of rGO and rGO/CQDs-HP were recorded by using the FESEM (MERLIN Compact with GEMINI I electron column, Zeiss India Pvt. Ltd.) with an acceleration voltage of 5kV. The Raman data was collected from Renishaw in Via Raman microscope at Laser wavelength of 514 nm. The UV-Visible (UV-Visible Spectrophotometer, Schimadzu, UV-2600), and fluorescence emission data (HORIBA JOBIN YVON Spectrofluorometer 4XP) were recorded to study the optical

behaviour of the CQDs-HP samples. The elemental analysis was carried out by performing X-ray photoelectron spectroscopy (XPS) analysis (SI. No.10001.Prevac.Poland) equipped with an Al-Kα monochromatic source (1486.6 eV). All the electrochemical supercapacitor measurements were carried out by Bio-logic instrument (EC.Lab, V: 10.37) using a Swagelok type two electrode fitting. The electrochemical measurements for oxygen reduction were carried out by CHI-660C electrochemical workstation using three electrode systems.

Electrode preparation

The electrode preparation for the supercapacitor testing was carried out by using a Swagelok type two-electrode cell. In the fitting, two stainless steel electrodes (12.7 mm diameter) were used. The well grinded powdered sample gets dispersed in ethanol by ultrasonication and drop casted onto the electrode surface. The electrodes were dried in a vacuum desiccator for prior use. A cellulose nitrate membrane soaked in 1M Na_2SO_4 was placed as separator between the electrodes fitted with Swagelok type two electrodes setting. All the measurements for supercapacitor testing were carried out with the Bio-Logic instrument with working potential window between -0.1 to 0.9V.

The oxygen reduction reaction (ORR) was performed by a two compartment three electrode system consisting of a bare platinum wire as the counter electrode, Ag/AgCl (3M NaCl) as the reference and a glassy carbon (GC) as the working electrode. Prior to each electrochemical measurement, the GC electrode was sequentially polished by aqueous alumina slurry (0.05 µm, Buehler) followed by repeated sonication in deionised water to get a mirror finish surface. The well-cleaned electrodes were dried in an argon gas flow and used for modification with the samples. In a typical procedure, a mixture of 5% nafion and the as-synthesized samples (rGO and rGO/CQDs-HP) was prepared and drop casted onto the GC electrode followed by vacuum drying. Then, the modified GC electrodes were taken to study their electrocatalytic activity towards the ORR in oxygen saturated 0.1M KOH solution using CHI-660C electrochemical workstation. The rotating disc electrode (RDE) measurements were carried out to observe the ORR activity of the samples and the involved reaction kinetics. For this purpose, the rotating disc electrodes (RDE) were modified with samples by following the procedure as used for the GC electrode. Then the linear sweep voltammetry (LSV) data was collected at 10 mV/s sweep rate with 100-1600 rpm using RDE Pine instruments, USA attached to the CHI-660C electrochemical workstation. The electrochemical impedance measurement was carried out at a signal of 5mV amplitude within the frequency range of 0.1 MHz to 0.1 Hz and is presented in the Nyquist plot (real impedance vs. imaginary impedance).

Results and discussion

The GO was synthesized from the graphite by following the modified Hummer's method and successfully characterized by different techniques. The reduced graphene oxides (rGO) was prepared from GO by hydrothermal process. The success in reduction process was verified by UV-visible spectral measurement. The preliminary UV-visible spectrum of GO and rGO were collected by dispersing the samples in deionised water by ultrasonication (Fig. S1†). The GO gives one prominent peak at 230 nm and a small shoulder peak at 290 nm assigned for π-π* and n-π* electronic transitions respectively indicating the existence of both C=C and C=O functional groups.[3b,19] After the reduction, the peak at 230 nm appeared for GO vanished which validate its conversion to rGO.[19] The peak at 230 nm shifted to 260 nm further showing the restoration of aromatic conjugated systems in rGO.[3b] The CQDs co-doped with S and N was synthesized by a facile single step hydrothermal route using protamine and heparin as the nitrogen and sulphur source respectively. To our belief, this is the first report in choosing the rich source of nitrogen and sulphur containing protamine and heparin, respectively for

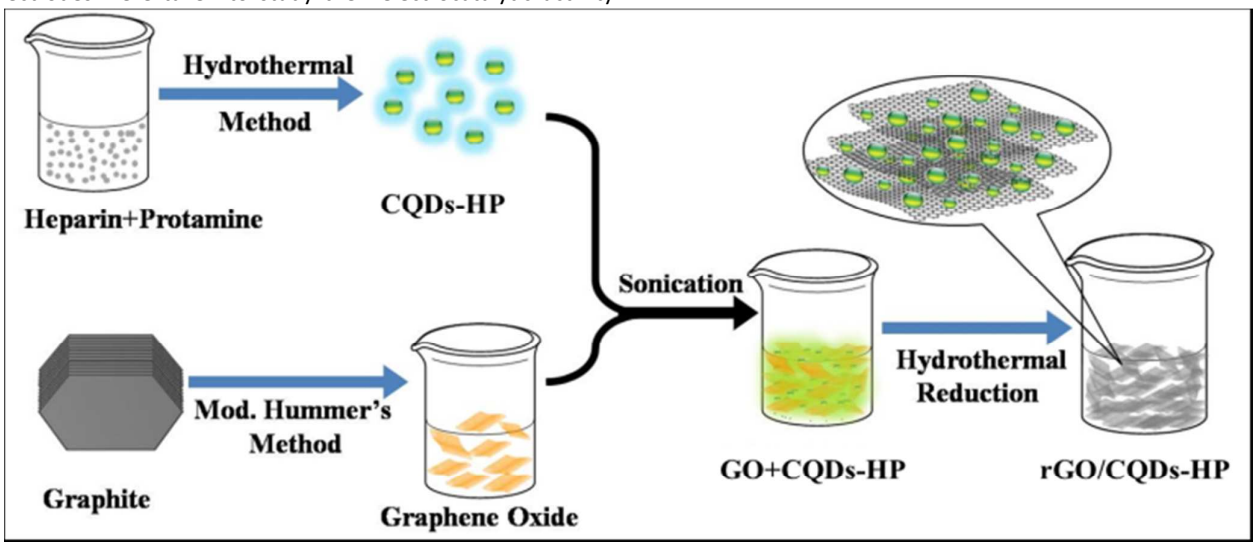

Scheme.1 Scheme represents the synthesis process for rGO/CQDs-HP hybrids.

synthesis of heteroatom doped CQDs. It is believed that under the high temperature and pressure exerted in the autoclave make the heparin and protamine molecule to undergo polymerisation and carbonisation producing the N, S co-doped CQDs.[20] The optical behaviour of the as-synthesized CQDs was studied with UV-Visible and photoluminescence spectral analysis. As it can be seen in Fig. S2†, the UV-Visible spectrum shows a hump like peak at 310 nm assigned to the n-π* electronic transition taking place on the surface of CQDs-HP.[21] The photoluminescence emission spectrum for CQDs-HP appeared at 410 nm when excited at 330 nm (Fig. S2†). Furthermore, the CQDs-HP emits bright blue colour under 365 nm UV-lamp exposures (inset of Fig. S2†). It is clearly observed that under UV light illumination the CQDs-HP solution emits bright blue colour fluorescence. Similarly the UV-visible spectra for the CQDs-HP (1:2) and CQDs-HP (2:1) were recorded to deduce any effect of amounts of reactants on the synthesis of CQDs (Fig. S3†). The UV-Visible spectra of different CQDs showed a hump like peak. interestingly, on changing the variation of the reactant ratio, the peak positions of CQDs got shifted. In the case of CQDs-HP and CQDs-HP (1:2), the hump like peaks arises in the range of 310 to 315 nm but the CQDs-HP (2:1) shows a blue shift in the peak position to 272 nm. This shifting in the peak position may be due to the variation in the surface functionality and the content of S and N heteroatom. Further, the steady state photoluminescence (PL) analysis reveals that all the CQD samples show the excitation dependent emission behaviour (Fig. S4†). The excitation dependent emission behaviour reveals the formation of different sizes of CQD particles.[11] Interestingly, the emission maximum for different CQD arises at different excitation wavelength. This observation reveals the impact of variation of the content of starting reactants on the UV-visible and Photoluminescence behaviour. All the CQDs sample emit bright blue colour under 365 nm UV-lamp exposures. The elemental composition of CQDs-HP was estimated from the X-ray photoelectron spectroscopy (XPS) analysis. The full spectrum survey of CQDs-HP indicates the presence of nitrogen (N) and sulphur (S) along with the carbon and oxygen atoms (Fig. S5†). The close observation of the hi-resolution deconvolution XPS spectrum of C1s shows the presence of C=C (284 eV), C-C/C-H (285.1 eV), C-OH/C-N/C-S (286.2 eV), C-O-C (287.5 eV), C=O (289 eV) functional groups.[3b,14a] The deconvolution of the N1s spectrum suggested the presence of three types of nitrogen functional groups as pyridinic (399.2 eV), pyrrolic (400.4 eV) and graphitic nitrogen (401.6 eV) domains.[5a,14a] The existence of sulphur in various oxidation states (167.7, 168.5, 169.5 eV) was also verified from the hi-resolution deconvolution XPS spectrum of S2p.[13b] The presence of S to N ratio has been estimated to be to be 1:5.

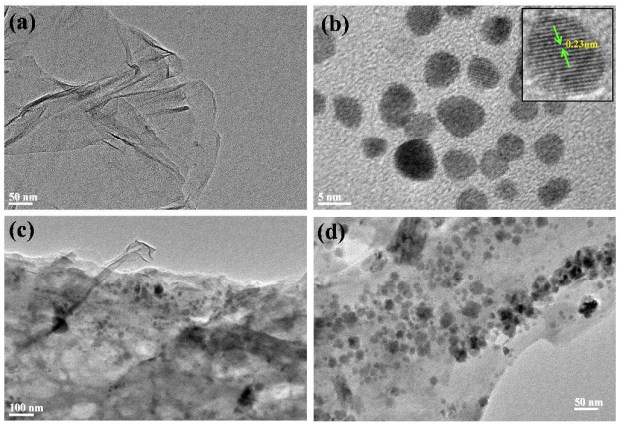

Figure 1. TEM images of rGO (a), CQDs-HP (b) and rGO/CQDs-HP (c, d). The insert image in b shows the HRTEM image of CQDs-HP.

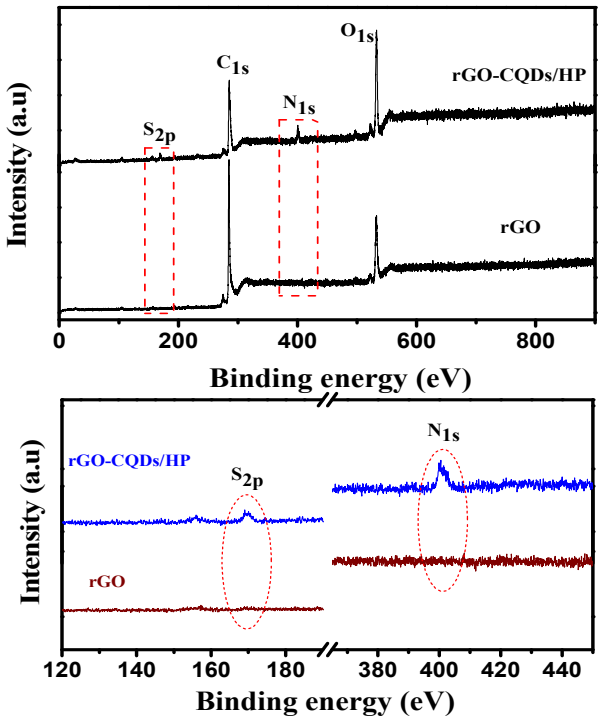

Figure 2. XPS spectrum of rGO and rGO/CQDs-HP

The rGO and CQDs/HP composites (rGO/CQDs-HP) were prepared by the hydrothermal procedure as represented in Scheme 1. The FESEM and TEM study was carried out to know the morphology of the as-synthesized rGO, CQDs-HP and rGO/CQDs-HP composites. As it can be seen (Fig. S6†), a random arrangement of layers in a 3D network like features was observed in rGO. In case of rGO/CQDs-HP composite, although the 3D arrangement is found, but the graphene sheets are highly consistent and arranged as layer by layer in an orderly manner making increase in the surface area with accessible regular smooth interspaces. TEM images of rGO reveals that the sheets are very much transparent in nature and well dispersed with folding around (Fig. 1). On the other hand, the as-synthesized CQDs-HP particles are found to be more disperse and spherical in shape. The average size of the particles was calculated to be 3.7 nm. The hi-resolution TEM images elucidate the well-resolved interlayer spacing of 0.23nm, which is close to the (100) facet of graphite.[11a] In rGO/CQDs-HP, the CQDs-HP particles are well decorated

throughout the graphene sheets. The CQDs-HP particles were also inserted between the graphene sheets leading a sandwich-like structure and formed agglomerates. While, inside the solution, the CQDs are well dispersed with uniform size distributions, but these are got agglomerated when sandwiched with graphene during the drying process. This sandwiched CQDs-HP served as interlayer spacer to prevent the restacking of the sheets after reduction.[22] This may help to increase the surface area of the graphene and make accessible to ions for capacitance enhancement.

The elemental composition of the samples were analysed by X-ray photoelectron spectroscopy (Fig. 2). In the full spectrum of rGO, the peaks at 284.6 and 530 eV indicate the presence of the carbon skeleton and oxygen functionalities. In the case of rGO/CQDs-HP composite, along with the peaks at 284.6 and 530 eV, two additional characteristic peaks were observed at 169.6 and 400.5 eV, showing the presence of both Sulphur (S) and Nitrogen (N) atoms in the sp^2 carbon skeleton. The deconvolution of the high-resolution C1s and N1s peaks (Fig. S7†) was carried out by using a Gaussian peak shape followed by the background correction. The peak at 284.6, 286.1 eV of C1s are assigned to the C=C and C-OH bonding. The less intense peaks at 287.2 and 288.5 eV are for the presence of oxygen-containing other functional groups.[3b,14a] Further, the high-resolution XPS spectrum of N1s was taken to know the type of nitrogen atoms present in the sample. The deconvolution of this spectrum suggested the presence of three types of nitrogen functional groups as pyridinic (399.2 eV), pyrrolic (400.4 eV) and graphitic nitrogen (401.6 eV) domains.[5a,14a] The high resolution deconvolated XPS spectrum for the S2p depicts the presence of three peaks at 164.5, 167.5 and 168.6 eV that are attributed for the S $2p_{½}$ of thiophene (C-S-C) and the oxidised sulphur groups (-C-SOx bonding, x= 2-4).[13b,23] Further, the atomic ratio of carbon to oxygen (C/O) was estimated from XPS analysis. It was found to be 1.64 and 0.63 for rGO and rGO/CQDs-HP samples respectively. Also, the ratio of the area under the deconvolated curve for C=C/C-C to C-O was analysed. It was estimated to be 2.90 and 1.65 for rGO and rGO/CQDs-HP respectively. This reveals the higher oxygen content in rGO/CQDs-HP composite as compared to the rGO. This may be contributed from oxygen functional groups of the CQDs-HP particles present in between the graphene sheets. Thus, the XPS analysis reveals that the rGO/CQDs-HP composite contains mainly the C and O atoms along with the N and S atoms in the form of pyridinic, pyrrolic, graphitic nitrogen and thiophene like structures within the carbon framework.

Further, the Raman measurements were carried out to explore the status of structural disorders taking place during the conversion of GO to rGO and formation rGO/CQDs-HP.[3b,24] The data are presented in Fig. S8†. The Raman spectra show two characteristic peaks at 1356.8 cm^{-1} at 1591.3 cm^{-1} denoted as D and G band respectively. The D-band is assigned to the breathing mode of k-point photons of A1g symmetry, and the G-band corresponds to the 1st order scattering of the E2g phonon of sp^2 carbon atoms. It has been observed that the intensity of D-band is very much sensitive towards the structural changes in graphene frame.[10a] Therefore, the

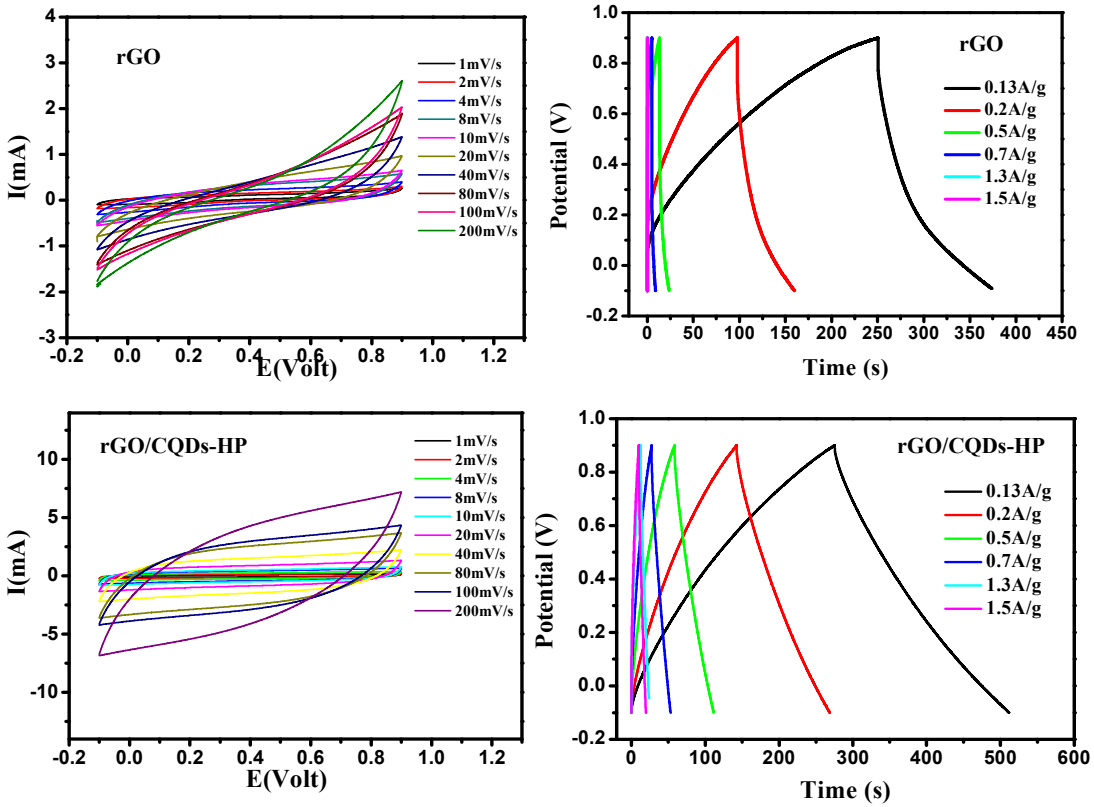

Figure 3. Cyclic voltamograms of rGO and rGO/CQDs-HP at different scan rates and the GCD profiles at the corresponding current densities.

intensity ratio of D-band and G-band (I_D/I_G) was estimated from Raman signal of GO, rGO, rGO/CQDs-HP. Here, an increase in I_D/I_G is observed from GO (0.86) to rGO (0.89). This observation validates the formation of a more number of small size sp^2 domains in the graphene frame.[3b,8b] This confirms the successful reduction of GO to rGO during this synthesis process. Further, an increase in I_D/I_G was observed for rGO/CQDs-HP (0.95) compared to rGO. This suggests the addition more defects in the rGO/CQDs-HP due to the insertion of heteroatom (N, S) in the carbon skeleton.[10c,25]

The interesting arrangement of CQD-HPs within the interlayer of rGO may expect to enhance the accessible for charged ions to increase the capacitance of composites. This observation attracted to explore the supercapacitor performance of rGO/CQDs-HP composites. Therefore, asymmetrical supercapacitor arrangement for real applications was carried out by using the stainless steel two electrode systems by placing a cellulose nitrate membrane as a separator as shown in Fig. S9†. The cyclic voltammetry (CV) and galvanic charge-discharge (GCD) measurements are made to evaluate their capacitance values. The CV measurements were recorded for both rGO and rGO/CQDs-HP composites at different scan rates with similar potential window of 1V. As it can be seen from Fig. 3, In case of rGO/CQDs-HP the shape of the CV profiles are of nearly rectangular compared to rGO, showing a better choice for supercapacitor application.[15,26] The capacitance value was calculated from CV profile using equation 1†. Interestingly, the rGO/CQDs-HP shows a higher capacitance value of 156 F/g which is 1.6 times higher than the value obtained for rGO (98 F/g). The GCD experiment was also carried out to support the results obtained from the CV. Interestingly, the charge-discharge (CD) profile curves are symmetrical in nature at different applied current densities, revealing it as an ideal material for electrolytic double layer capacitors (Fig. 3).[27] From the GCD data, the specific capacitance was calculated by following the equation 2† and was found to be 141 F/g and 92.8 F/g for rGO/CQDs-HP and rGO respectively. This signifies the higher capacitance retention of rGO/CQDs-HP due to the presence of CQDs as spacer between the rGO layers. In order to verify the impact of ratios of CQDs in rGO/CQDs-HP, the supercapacitor measurements have been carried out. The cyclic voltammetry (CV) and charge-discharge (CD) measurement for all the rGO/CQDs-HP composites at different ratio are recorded. The variation of the CQDs-HP ratio in rGO changes the CV and CD patters (Fig. S10†). The rGO/CQDs-HP (1:2) and rGO/CQDs-HP (2:1) shows a capacitance value of 196 and 102 F/g respectively. Interestingly, on increasing the content of CQDs-HP in rGO, the capacitance value increases. The enhanced capacitance of rGO/CQDs-HP (1:2) may be due to presence of

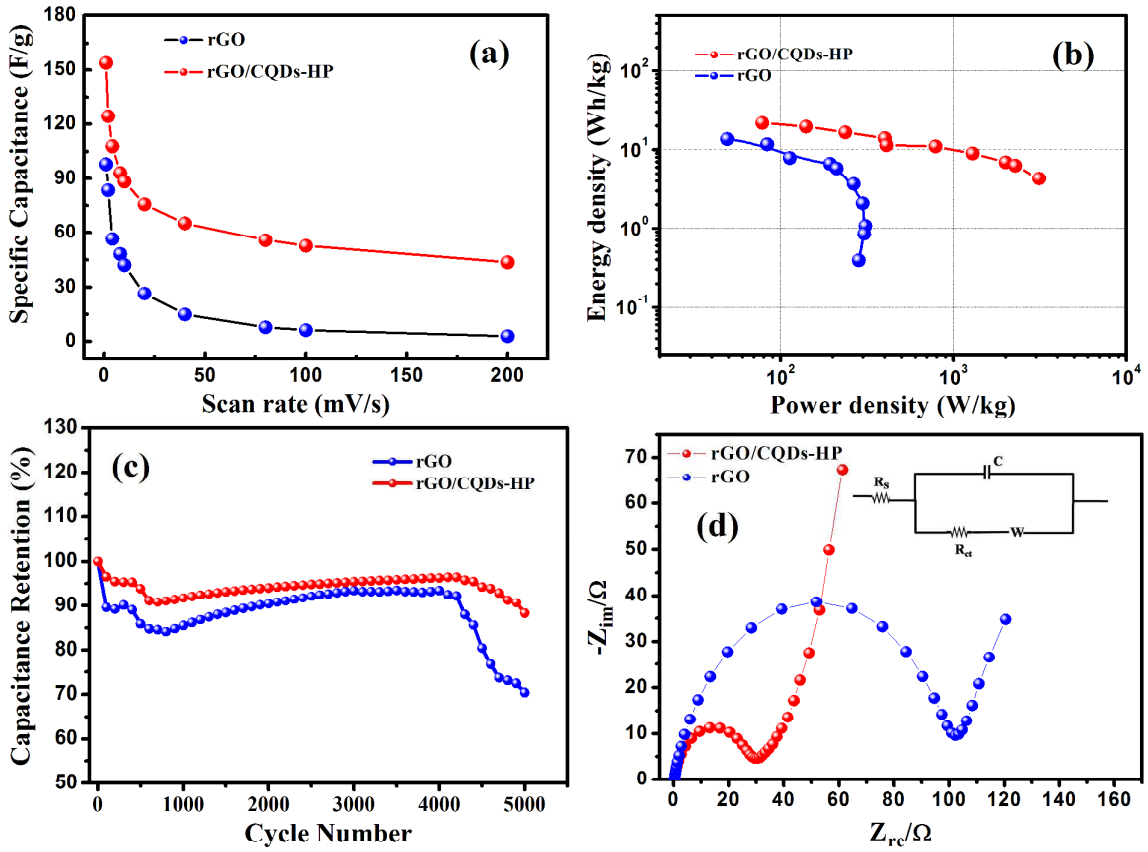

Figure 4. (a) Plot of specific capacitance retention vs. scan rate, (b) the Ragone plot at different scan rates, (c) plot of capacitance retention at various cycles for rGO and rGO/CQDs-HP and (d) Nyquist plot of rGO and rGO/CQDs-HP (the inset is the corresponding circuit diagram).

more CQDs-HPs which plays as spacer and provide more access for diffusion of charged ions in the interlayer of rGO.

Further, the capacitance of the materials was calculated from CV profile at different scan rate (Fig. 4a). Interestingly, the capacitance value decreases on increasing the scan rate. This observation can attributed that on increasing the scan rate the diffusion of charged ions decreases which reflects a fall in the capacitance.[28] Hou et al. have observed similar pattern for the asymmetric pseudo capacitor based on the polypyrrole/MnO_2 supported on nanoporous gold electrode.[29] Further, the energy density (ED) and power density (PD) were calculated (equation 3 and 4†) from the capacitance results of rGO and rGO/CQDs-HP. The Ragone plot of ED versus PD is made at different scan rates presented in Fig. 4b. From the plot, the ED and PD of rGO/CQDs-HP were found to be 21.7 $WhKg^{-1}$ and 78.12 WKg^{-1} respectively which is higher than the rGO (13.61 WhKg-1 and 49 WKg^{-1}) at scan rate of 1 mV/s. It is worthy to point here that the rGO/CQDs-HP shows high value of ED as compared to the values recently documented for graphene oxides, polyaniline network on Au coated conventional printing papers and etc.[30] The cyclic stability test is an important parameter for practical application of supercapacitors. In this work, the cycling performance test of the rGO and rGO/CQDs-HP was verified with CV measurement of the as modified two electrode arrangements. The capacitance values are estimated at 200 mV/s scan rate with repeated cycles and compared thereof with the initial cycle (Fig. 4c). The rGO/CQDs-HP modified electrode shows 90% retention of its initial specific capacitance after 5000 cycles whereas the only rGO shows 70%. This value indicates excellent long term capacitance retention stability of the rGO/CQDs-HP over rGO. This high specific capacitance and ED/PD value of rGO/CQDs-HP is believed due to the beneficial role of CQDs-HP and the synergistic role of both rGO and CQDs-HP in the composite. The CQDs-HPs may play as spacer and provide the access for diffusion of charged ions in the interlayer of rGO. The large surface to volume ratio of rGO may allow more active surfaces for ion adsorption. Thus, the synergistic role of both rGO and CQDs-HP contributes the high performance super capacitance behaviour of rGO/CQDs-HP. Although the super capacitance properties of graphene and its metal oxides hybrids have been well documented, only few report explored the super capacitance behaviour of CQDs. The point should be noted here that this is the first observation portraying the combining effect of both the doped CQDs and graphene in enhancing the super capacitance properties. So the excellent capacitance properties of rGO/CQDs-HP can be attracted to utilise as efficient material in supercapacitor development for practical applications in various fields of interest. It has been observed that the power output capability of the supercapacitor materials is strongly dependent on charge propagation due to the diffusion ions through the materials. This can be estimated from the electrochemical impedance behaviour of the materials.[28c] The internal resistance of the supercapacitors plays the vital role in operation rate of a capacitor that can be estimated from the Nyquist plot of impedance. Therefore, the electrochemical impedance spectroscopy (EIS) measurements were carried out for rGO/CQDs-HP to validate their supercapacitor applications. Here, the net impedance obtained is the sum of solution resistance (Rs) and the charge transfer resistance of materials (Rct).[31] In this study, the EIS measurements for rGO and rGO/CQDs-HP were carried out at same electrode arrangements and experiment conditions. Hence, the variation in the impedance value must be due to the difference in the internal resistance of electrode materials. The Nyquist impedance data of rGO and rGO/CQDs-HP show semicircle type behaviour in the high-frequency region (Fig. 4d). The diameter of the semicircle yields the charge transfer resistance (Rct) of the materials at electrolyte interface.[28b,29c,32] It can be clearly seen that the rGO shows a semicircle of comparatively higher diameter (Rct = 95.1Ω) as compared to the rGO/CQDs-HP (Rct=28 Ω). This indicates that rGO/CQDs-HP has significant lower resistance in charge propagation at the interface between the electrode/electrolyte than the rGO that justify its higher power output capability. So, it can be attracted for promising applications in supercapacitors development.

It is well known that, the novel metal nanoparticles were broadly used towards the development of electrocatalyst for designing the PEM fuel cells. But their high market value and limited availability confines their application for which an alternative metal free electrode material is highly desired.[3b,14b,33] Although the carbon based electrode materials as nanotubes, graphene, activated carbon etc. are been adopted as the alternative to the metal catalysts, but their activity is not par for practical application. Therefore, they need substantial modifications to improve their properties. Interestingly, the modification of the carbon nanomaterials with heteroatom like, N, S, etc. enhances their electrocatalytic behaviour towards the ORR and seems to be nearly approaching the activity of metal based catalysts.[14b] Along with the interesting optical properties of the recently discovered CQDs, the facile doping with hetero atoms attracts substantial attention towards excellent electrocatalytic activity for ORR applications. Attracted by the impressive structure

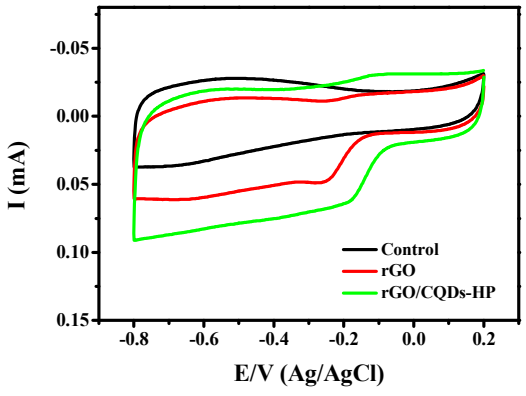

Figure 5. Cyclic voltamograms of ORR by rGO and rGO/CQDs-HP in oxygen saturated 0.1M KOH electrolyte. The control experiment was carried out in argon saturated 0.1M KOH. Scan rate: 10 mV/s

and presence of electron rich heteroatom (N and S co-doped) in rGO/CQDs-HP composites, the electrocatalytic activity has been explored towards oxygen reduction reaction. Fig. 5 depicts the cyclic voltamograms of rGO and rGO/CQDs-HP modified glassy carbon electrodes towards the reduction of oxygen in 0.1M KOH at a scan rate of 10mV/s. The rGO/CQDs-HP modified electrode catalyse the reduction of oxygen at higher positive potential (-0.17 V) and possess higher current efficiency compared to rGO. Interestingly, the onset potential for the reduction of oxygen on rGO/CQDs-HP modified electrode is 0.02V that 80 mV higher potential compared to rGO. This observation depicts the high-performance of rGO/CQDs-HP towards ORR application compared to its rGO counterparts. This can be ascribed due to the contribution of electron rich heteroatom doped CQDs as well as the synergistic effect of both CQDs and rGO for electrocatalytic reduction of oxygen. The contribution of CQDs can be explained as the content of electron rich atoms on it results a variation of electronegativity of rGO/CQDs-HP surface and produce more charged sites which are the favourable sites for the adsorption of oxygen molecules for reduction.[13b14b,34] Also the effect of CQDs-HP ratio in rGO/CQDs-HP composite towards the ORR has been verified. The as-synthesized rGO/CQDs-HP (1:2) and rGO/CQDs-HP (2:1) were employed as the electrode material and the CV data for ORR were recorded at similar conditions (Fig. 11†). It clearly shows that in case of rGO/CQDs-HP (1:2) the onset and reduction potential of ORR was found to be close to that of rGO/CQDs-HP, whereas for rGO/CQDs-HP (2:1) sample it was close to the rGO. It clearly depicts that the content of CQDs-HP plays the vital role for catalytic reduction of oxygen. However, on further increased content of CQDs-HP in the rGO/CQDs-HP composites does not affect appreciably on the catalytic performance of the rGO/CQDs-HP for ORR.

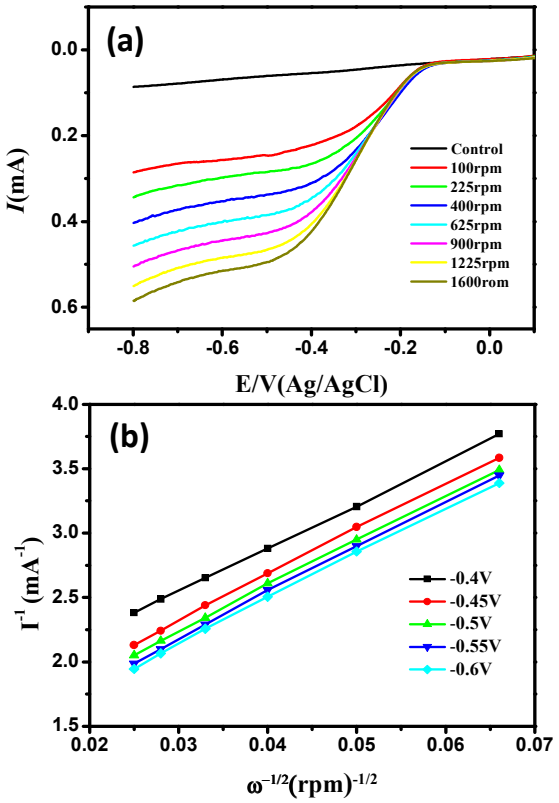

Figure 6. (a) RDE voltamograms of rGO/CQD-HP at different rpm and (b) the corresponding Koutecky-Levich plots for O_2 reduction in 0.1M KOH. Scan rate: 10 mV/s.

Further, the reaction kinetics involved in the ORR process on rGO/CQDs-HP modified electrode was evaluated by measuring the limiting current at various electrode rotation rates (Fig. 6). It was observed that on increasing the rotation rate of the electrode the reduction current goes on increasing that is due to the increased diffusion of the electrolyte.[14a,35] The mechanism of the reaction was studied by calculating the number of electrons involved in the reduction process using the Koutecky-Levich (K-L) equation (equation 6†). The KL plot corresponding to the linear sweep voltages at different potentials is presented in Fig. 6b. In this plot, the parallel and straight linear fitting indicates the first order reaction kinetics respect to the dissolved oxygen. The calculated value of n is ranging from 3.5- 3.75 nearly equal to 4, suggesting the four-electron reduction process for ORR on rGO/CQDs-HP (Fig. 6b) and the O_2 get directly converted to OH^-. The point should be noted here that the present materials avoid the generation of H_2O_2 as intermediates in two-electron reduction process of ORR which damage the carbon based catalyst.[36] These results indicate that, the as developed rGO/CQDs-HP can be used as the better electrocatalyst for ORR in PEM fuel cells.

Conclusions

In summary, we have presented here a facile, single step green synthetic method for producing rGO/CQDs-HP having a 3D sandwich-like structure. The CQDs-HP particles are found to be acts as a spacer, preventing the restacking of the graphene layers after reduction. The as-synthesized composite exhibits a high specific capacitance of 156 F/g having a robust cyclic stability (90% capacitance retention) after 5000 cycles with high energy and power density (22.4 $WhKg^{-1}$ and 76.68 WKg^{-1} respectively) in comparison to its rGO counterparts. Moreover, the rGO/CQDs-HP shows good electrocatalytic behaviour for the reduction of oxygen. This report provides a scope to produce the graphene-based composites towards development of supercapacitor materials, as well as the electrode material for PEM fuel cell through an easy and facile route.

Acknowledgements

The Authors are grateful to Prof. B. K. Mishra, Director CSIR-IMMT for his kind permission and encouragement for doing this study. Dr. B. K Jena acknowledges BRNS, Mumbai, India (No.2013/37p/67/BRNS) and MNRE, New Delhi, India (No.102/87/2011-NT) for the financial support. AKS and SCS

acknowledge CSIR, India for the fellowship. The authors are thankful to Dr. B.P. Bag for PL measurements, and Mr. A. Dash and Prof. P. V. Satyam for TEM measurements.

Notes and references

1 (a) Y. Zhu, S. Murali, M. D. Stoller, K. J. Ganesh, W. Cai, P. J. Ferreira, A. Pirkle, R. M. Wallace, K. A. Cychosz, M. Thommes, D. Su, E. A. Stach and R. S. Ruoff, *Science*, 2011, **332**, 1537; (b) L. F. Chen, Z. H. Huang, H. W. Liang, W. T. Yao, Z. Y. Yu and S. H. Yu, *Energy Environ. Sci.*, 2013, **6**, 3331; (c) Y. Xu, Z. Lin, X. Huang, Y. Liu, Y. Huang and X. Duan, *ACS Nano*, 2013, **7**, 4042; (d) X. Wang, W. Song, B. Liu, G. Chen, D. Chen, C. Zhou and G. Shen, *Adv. Funct. Mater.*, 2013, **23**, 1202; (e) C. Zhang, H. Yin, M. Han, Z. Dai, H. Pang, Y. Zheng, Y. Q. Lan, J. Bao, and J. Zhu, *ACS Nano*, 2014, **8**, 3761.

2 (a) S. Faraji and F. N. Ani, *J. Power Sources*, 2014, **263**, 338; (b) D. Guo, Y. Luo, X. Yu, Q. Li and T. Wang, *Nano Energy*, 2014, **8**, 174; (c) P. Yang and W. Mai, *Nano Energy*, 2014, **8**, 274.

3 (a) Y. Kang, X. Ye, J. Chen, Y. Cai, R. E. Diaz, R. R. Adzic, E. A. Stach and C. B. Murray, *J. Am. Chem. Soc.*, 2012, **135**, 42; (b) S. C. Sahu, A. K. Samantara, B. Satpati, S. Bhattacharjee and B. K. Jena, *Nanoscale*, 2013, **5**, 11265; (c) R. Choi, S. I. Choi, C. H. Choi, K. M. Nam, S. I. Woo, J. T. Park and S. W. Han, *Chem. Eur. J.*, 2013, **19**, 8190.

4 D. Jariwala, V. K. Sangwan, L. J. Lauhon, T. J. Marks and M. C. Hersam, *Chem. Soc. Rev.*, 2013, **42**, 2824.

5 (a) J. Jin, F. Pan, L. Jiang, X. Fu, A. Liang, Z. Wei, J. Zhang and G. Sun, *ACS Nano*, 2014, **8**, 3313; (b) Y. Huang, J. Liang and Y. Chen, *Small*, 2012, **8**, 1805.

6 (a) M. J. Allen, V. C. Tung and R. B. Kaner, *Chem. Rev.*, 2009, **110**, 132; (b) J. Zhao, Z. Wang, J. C. White and B. Xing, *Environ. Sci. Technol.*, 2014, **48**, 9995; (c) S. Eigler and A. Hirsch, *Angew. Chem. Int. Ed.*, 2014, **53**, 7720; (d) S. Guo and S. Dong, *Chem. Soc. Rev.*, 2011, **40**, 2644.

7 (a) G. Han, Y. Liu, L. Zhang, E. Kan, S. Zhang, J. Tang and W. Tang, *Sci. Rep.*, 2014, **4**; (b) Q. Guan, J. Cheng, B. Wang, W. Ni, G. Gu, X. Li, L. Huang, G. Yang and F. Nie, *ACS Appl. Mater. Interfaces*, 2014, **6**, 7626; (c) M. Yang, Y. Zhong, L. Su, J. Wei, and Z. Zhou, *Chem. Eur. J.*, 2014, **20**, 5046; (d) S. C. Sahu, A. K. Samantara, A. Dash, R. R. Juluri, R. K. Sahu, B. K. Mishra and B. K. Jena, *Nano Res.*, 2013, **6**, 635.

8 (a) Y. Zheng, Y. Jiao, L. Ge, M. Jaroniec and S. Z. Qiao, *Angew. Chem. Int. Ed.*, 2013, **52**, 3110; (b) D. Wei, Y. Liu, Y. Wang, H. Zhang, L. Huang and G. Yu, *Nano Lett.*, 2009, **9**, 1752; (c) L. Qu, Y. Liu, J. B. Baek and L. Dai, *ACS Nano*, 2010, **4**, 1321; (d) X. Wang, X. Li, L. Zhang, Y. Yoon, P. K. Weber, H. Wang, J. Guo and H. Dai, *Science*, 2009, **324**, 768.

9 (a) T. Xing, Y. Zheng, L. H. Li, B. C. C. Cowie, D. Gunzelmann, S. Z. Qiao, S. Huang and Y. Chen, *ACS Nano*, 2014, **8**, 6856; (b) H. Wang, M. Xie, L. Thia, A. Fisher and X. Wang, *J. Phys. Chem. Lett.*, 2013, **5**, 119; (c) H. Wang, T. Maiyalagan, and X. Wang, *ACS Catal.* 2012, **2**, 781; (d) L. Lai, J. R. Potts, D. Zhan, L. Wang, C. K. Poh, C. Tang, H. Gong, Z. Shen, J. Lin and R. S. Ruoff, *Energy Environ. Sci.*, 2012, **5**, 7936; (e) Q. Li, S. Zhang, L. Dai and L. Li, *J. Am. Chem. Soc.*, 2012, **134**, 18932; (f) S. M. Unni, S. N. Bhange, R. Illathvalappil, N. Mutneja, K. R. Patil and S. Kurungot, *Small*, 2014, **11**, 352.

10 (a) Z. Lin, G. H. Waller, Y. Liu, M. Liu and C. Wong, *Nano Energy*, 2013, **2**, 241; (b) Y. Wang, Y. Shao, D. W. Matson, J. Li and Y. Lin, *ACS Nano*, 2010, **4**, 1790; (c) H. M. Jeong, J. W. Lee, W. H. Shin, Y. J. Choi, H. J. Shin, J. K. Kang and J. W. Choi, *Nano Lett.*, 2011, **11**, 2472.

11 (a) S. Baker and G. Baker, *Angew. Chem. Int. Ed.*, 2010, **49**, 6726; (b) C. Ding, A. Zhu and Y. Tian, *Acc. Chem. Res.*, 2013, **47**, 20.

12 (a) S. Kim, S. W. Hwang, M. K. Kim, D. Y. Shin, D. H. Shin, C. O. Kim, S. B. Yang, J. H. Park, E. Hwang, S. H. Choi, G. Ko, S. Sim, C. Sone, H. J. Choi, S. Bae and B. H. Hong, *ACS Nano*, 2012, **6**, 8203; (b) L. Cao, X. Wang, M. J. Meziani, F. Lu, H. Wang, P. G. Luo, Y. Lin, B. A. Harruff, L. M. Veca, D. Murray, S. Y. Xie and Y. P. Sun, *J. Am. Chem. Soc.*, 2007, **129**, 11318; (c) X. Guo, C. F. Wang, Z. Y. Yu, L. Chen and S. Chen, *Chem. Commun.*, 2012, **48**, 2692; (d) H. Li, X. He, Z. Kang, H. Huang, Y. Liu, J. Liu, S. Lian, C. H. A. Tsang, X. Yang and S. T. Lee, *Angew. Chem. Int. Ed.*, 2010, **49**, 4430.

13 (a) H. Jiang, Y. Zhu, Q. Feng, Y. Su, X. Yang and C. Li, *Chem. Eur. J.*, 2014, **20**, 3106; (b) Z. L. Wu, P. Zhang, M. X. Gao, C. F. Liu, W. Wang, F. Leng and C. Z. Huang, *J. Mater. Chem. B*, 2013, **1**, 2868; (c) S. Liu, J. Tian, L. Wang, Y. Zhang, X. Qin, Y. Luo, A. M. Asiri, A. O. Al-Youbi and X. Sun, *Adv. Mater.*, 2012, **24**, 2037.

14 (a) Y. Li, Y. Zhao, H. Cheng, Y. Hu, G. Shi, L. Dai and L. Qu, *J. Am. Chem. Soc.*, 2011, **134**, 15; (b) H. Fei, R. Ye, G. Ye, Y. Gong, Z. Peng, X. Fan, E. L. G. Samuel, P. M. Ajayan and J. M. Tour, *ACS Nano*, 2014, **8**, 10837; (c) C. Hu, C. Yu, M. Li, X. Wang, Q. Dong, G. Wang and J. Qiu, *Chem. Commun.*, 2015, **51**, 3419.

15 W. W. Liu, Y. Q. Feng, X. B. Yan, J. T. Chen and Q. J. Xue, *Adv. Funct. Mater.*, 2013, **23**, 4111.

16 (a) Y. Zhu, X. Ji, C. Pan, Q. Sun, W. Song, L. Fang, Q. Chen and C. E. Banks, *Energy Environ. Sci.*, 2013, **6**, 3665; (b) L. Lv, Y. Fan, Q. Chen, Y. Zhao, Y. Hu, Z. Zhang, N. Chen and L. Qu, *Nanotechnology*, 2014, **25**, 235401; (c) Y. Hu, Y. Zhao, G. Lu, N. Chen, Z. Zhang, H. Li, H. Shao and L. Qu, *Nanotechnology*, 2013, **24**, 195401.

17 Q. Chen, Y. Hu, C. Hu, H. Cheng, Z. Zhang, H. Shao and L. Qu, *Phys. Chem. Chem. Phys.*, 2014, **16**, 19307.

18 (a) W. S. Hummers and R. E. Offeman, *J. Am. Chem. Soc.*, 1958, **80**, 1339; (b) G. Goncalves, P. A. A. P. Marques, C. M. Granadeiro, H. I. S. Nogueira, M. K. Singh and J. Grácio, *Chem. Mater.*, 2009, **21**, 4796.

19 S. C. Sahu, A. K. Samantara, M. Seth, S. Parwaiz, B. P. Singh, P. C. Rath and B. K. Jena, *Electrochem. commun.*, 2013, **32**, 22.

20 (a) P. C. Hsu and H. T. Chang, *Chem. Commun.*, 2012, **48**, 3984; (b) X. Jia, J. Li and E. Wang, *Nanoscale*, 2012, **4**, 5572.

21 (a) J. Peng, W. Gao, B. K. Gupta, Z. Liu, R. Romero-Aburto, L. Ge, L. Song, L. B. Alemany, X. Zhan, G. Gao, S. A. Vithayathil, B. A. Kaipparettu, A. A. Marti, T. Hayashi, J. J. Zhu and P. M. Ajayan, *Nano Lett.*, 2012, **12**, 844; (b) J. Niu and H. Gao, *J. Lumin.*, 2014, **149**, 159.

22 L. Zhang and G. Shi, *J. Phys. Chem. C*, 2011, **115**, 17206.

23 H. R. Thomas, A. J. Marsden, M. Walker, N. R. Wilson and J. P. Rourke, *Angew. Chem. Int. Ed.*, 2014, **53**, 7613.

24 (a) F. Tuinstra and J. L. Koenig, *J. Chem. Phys.*, 1970, 53; (b) A. Kaniyoor and S. Ramaprabhu, *AIP Adv.*, 2012, **2**, 032183.

25 (a) D. Yu, L. Wei, W. Jiang, H. Wang, B. Sun, Q. Zhang, K. Goh, R. Si and Y. Chen, *Nanoscale*, 2013, **5**, 3457; (b) J. Xu, J. Shui, J. Wang, M. Wang, H. K. Liu, S. X. Dou, I. Y. Jeon, J. M. Seo, J. B. Baek and L. Dai, *ACS Nano*, 2014, **8**, 10920; (c) H. Wang, T. Maiyalagan and X. Wang, *ACS Catal.*, 2012, **2**, 781.

26 X. Xiao, T. Li, P. Yang, Y. Gao, H. Jin, W. Ni, W. Zhan, X. Zhang, Y. Cao, J. Zhong, L. Gong, W. C. Yen, W. Mai, J. Chen, K. Huo, Y. L. Chueh, Z. L. Wang and J. Zhou, *ACS Nano*, 2012, **6**, 9200.

27 (a) Z. Wen, X. Wang, S. Mao, Z. Bo, H. Kim, S. Cui, G. Lu, X. Feng and J. Chen, *Adv. Mater.*, 2012, **24**, 5610; (b) J. L. Shi, W. C. Du, Y. X. Yin, Y. G. Guo and L. J. Wan, *J. Mater. Chem. A*, 2014, **2**, 10830.

28 (a) W. Zhou, K. Zhou, X. Liu, R. Hu, H. Liu and S. Chen, *J. Mater. Chem. A*, 2014, **2**, 7250; (b) Y. H. Lin, T.Y. Wei, H. C.

Chien and S. Y. Lu, *Adv. Energy Mater.*, 2011, **1**, 901; (c) Y. Wei, H. Liu, Y. Jin, K. Cai, H. Li, Y. Liu, Z. Kang and Q. Zhang, *New J. Chem.*, 2013, **37**, 886.
29 Y. Hou, L. Chen, P. Liu, J. Kang, T. Fujita and M. Chen, *J. Mater. Chem. A*, 2014, **2**, 10910.
30 (a) L. Yuan, X. Xiao, T. Ding, J. Zhong, X. Zhang, Y. Shen, B. Hu, Y. Huang, J. Zhou and Z. L. Wang, *Angew. Chem. Int. Ed.*, 2012, **51**, 4934; (b) G. P. Pandey, S. A. Hashmi and Y. Kumar, *Energy Fuels*, 2010, **24**, 6644; (c) B. Fang and L. Binder, *J. Phys. Chem. B*, 2006, **110**, 7877; (d) W. Gao, N. Singh, L. Song, Z. Liu, A. L. M. Reddy, L. Ci, R. Vajtai, Q. Zhang, B. Wei and P. M. Ajayan, *Nat Nanotechnol.*, 2011, **6**, 496.
31 R. S. Hastak, P. Sivaraman, D. D. Potphode, K. Shashidhara and A. B. Samui, *Electrochim. Acta*, 2012, **59**, 296.
32 K. Zhang, L. L. Zhang, X. S. Zhao and J. Wu, *Chem. Mater.*, 2010, **22**, 1392.
33 D. W. Wang and D. Su, *Energy Environ. Sci.*, 2014, **7**, 576.
34 M. Favaro, L. Ferrighi, G. Fazio, L. Colazzo, C. Di Valentin, C. Durante, F. Sedona, A. Gennaro, S. Agnoli and G. Granozzi, *ACS Catal.*, 2014, **5**, 129.
35 K. Gong, F. Du, Z. Xia, M. Durstock and L. Dai, *Science*, 2009, **323**, 760.
36 G. Zhang, B. Y. Xia, X. Wang and X. W. (David) Lou, *Adv. Mater.*, 2014, **26**, 2408.

Table of contents: